The Formation History of Olympus Mons from Paleo-Topography

by

Lauren M. Jozwiak

Submitted to the Department of Earth, Atmospheric and Planetary Sciences

in Partial Fulfillment of the Requirements for the Degree of

Bachelor of Science in Earth, Atmospheric and Planetary Sciences

at the Massachusetts Institute of Technology

June 2011

Author__ Signature redacted _____
Department of Earth, Atmospheric and Planetary Sciences
May 6, 2011

Certified by_____ Signature redacted _____
Linda Elkins-Tanton
Thesis Supervisor

Accepted by___ Signature redacted _____
Samuel Bowring
Chair, Committee on Undergraduate Program

The Formation History of Olympus Mons from Paleo-Topography

By

Lauren M. Jozwiak

Submitted to the

Department of Earth, Atmospheric, and Planetary Science

May 6, 2011

In Partial Fulfillment of the Requirements for the Degree of

Bachelor of Science in Earth, Atmospheric, and Planetary Sciences

Abstract

The formation of the volcano Olympus Mons, is linked directly to the geodynamic history of both Tharsis, and Mars as a whole. We sought to constrain the bulk formation period using paleo-topographic evidence. On the northeastern edge of the flexural trough, we located a lava flow whose path is radically discordant with current down-slope directions, indicating entrenchment prior to large-scale flexural trough formation. To constrain the end of bulk formation, we used the aureole deposits that surround the flanks of Olympus Mons, and were a consequence of crustal fracture under the weight of Olympus. Applying crater retention age dating to images from THEMIS VIS and THEMIS IR, we proposed the bulk formation of Olympus Mons occurred between $3.67_{-0.10}^{+0.05}$ Ga and $3.53_{-0.28}^{+0.09}$ Ga.

Table of Contents

List of Tables and Figures

Tables:

Figures:

Acknowledgements

I would like to acknowledge my research advisor, Jeff Andrews-Hanna for his guidance and illuminating discussions. I would also like to thank my academic advisor Rick Binzel for his ready advice and aid, and Linda Elkins-Tanton for overseeing this project's completion; additionally, R. J. Isherwood for his collaboration during our research synthesis and conference presentation.

I. Introduction

1.1Background

Olympus Mons is a shield volcano located in the Tharsis region of Mars. Centered at 18.4°N 226°E, it stands 25km high and is the tallest volcano in the solar system. Despite being one of the most recognizable features on Mars, the age of Olympus Mons remains uncertain due to the difficulty of locating a suitable surface on which to carry out crater retention age dating. Most surfaces on a volcano and its surrounding environs are covered by lava flows; thus any calculated age for these areas would be the age of the last lava flow, but give no hint as to the initial age of the volcano. Current ages for the flanks, calderas, and immediate surroundings of Olympus Mons converge around 150Ma [Werner 2009]. Werner, however, postulates the Olympus Mons formed well before this time, perhaps before 3.6Ga, based on a significantly older lava flow near the Amazonis Planitia that could have originated from a proto-Olympus Mons, although this single flow is the only datum Werner provides to support an older history for Olympus Mons [Werner 2009]. As will be shown, this work supports the early Hesperian age proposed by Werner, and provides a constrained period for the bulk formation of Olympus Mons through the use of paleo-topography.

1.2 Motivation

The primary motivations for this research are the range of implications the data provided have for the geo-dynamic evolution of Mars. Establishing a timeline for the formation and subsequent activity of Olympus Mons provides valuable information about the onset and cessation of volcanism on Mars, and by extension, information about the Martian mantle. This work provides both a constrained formation period for Olympus Mons, and postulates a complete history of activity based on direct evidence, and on comparisons to the Hawaiian system. The understanding of Olympus Mons as a mantle plume volcano

can also yield information beneficial in understanding terrestrial mantle plume volcanoes. As Mars lacks plate tectonics, it can be used as a simplified example of mantle plume dynamics, giving information on the duration of activity, and the possibility of renewed activity after the initial plume has ceased. When presented at the Lunar and Planetary Science Conference in March of 2011, this work sparked intense discussion with its relation to the theory of aureole deposits formation, and in the general formation mechanisms of volcanic edifices.

1.3 Approach

The analytic approach to this research was to use paleo-topography as a means of establishing a formation period for Olympus Mons. Paleo-topography is the process of using topographic features to infer information about the prior conditions of a region [Liu and Gurnis, 2010]. This use of paleo-topography focused on regional slope directions, in particular the change in regional slope directions caused by the emplacement of a flexural trough around Olympus Mons.

A flexural trough is a bowl-shaped depression resulting from flexure of the lithosphere surrounding a localized area of high mass, analogous to the depression formed around an object placed on a trampoline. Prior to the formation of Olympus Mons, the region of the flexural trough and its edges likely had very different topography, and the crust was then subsequently warped to its present day position.

This research initially centered on finding geologic features that were discordant with the current topography — namely lava flows that do not flow in the present-day downhill direction. Using the observation that with only slight deviation, liquids will flow in the direction of highest slope, one can then infer that these lava flows were emplaced prior to the flexural trough and the region's current topographic profile. By crater counting these lava flows, one can determine an age before the flexural trough, and hence an age before Olympus Mons or at least before a significant portion of Olympus Mons was formed. Research on flexural modeling of the region to constrain the percent of Olympus Mons that could have

been present before the region's topography would have diverted the discordant lava flows was carried out by R.J. Isherwood and J. C. Andrews-Hanna (Colorado School of Mines). The flexural modeling work supports conclusions derived from the results of this research, and is thus presented in the discussion. To determine an age for the end of Olympus Mons bulk formation, one dates the aureole deposits, using the theory that aureole deposits were caused by mass crustal failure, to be further addressed in the discussion. The exact methods and results of these analyses will be detailed in subsequent sections of this work.

II. Methods

2.1 Flow Identification

The initial stage of research involved analysis of MOLA (Mars Orbiter Laser Altimeter) data—specifically the 44°N - 0°latitude, 180°E-270°E longitude MEGDR topography data set. The .img file was downloaded to ENVI image analysis software and then exported for viewing in ArcGIS. ArcGIS coordinate system was set to Mars 2000 and a red-blue color stretch was applied to the data (red indicating high topography, and blue low topography). Various hillshade profiles were created and overlaid with 30% transparency one at a time so as to allow easier identification of surface features, specifically lava flows. The most ideal hillshade, and the one most frequently used was a sun elevation of 15° and an azimuthal angle of 45°. The region surrounding the flexural trough of Olympus Mons was then inspected for lava flows. Several lava flows were identified, and of these, 5 were noted for use in the study—3 appearing discordant with the present day topography, and 2 non-deviant flows to be used as standards.

2.2 Flow Categorization

Once the 5 study flows were identified, they were further analyzed to determine the natural variance of Martian lava flows, in the case of the standards, and the degree of deviance, in the case of the discordant lava flows. The broad analyses performed were to establish the regional downhill direction and the XY-

deviance of flow from said direction, the difference in XZ-slope both in the direction of the lava flow and the regional downhill direction, analysis of XZ-slope across the top of the lava flow perpendicular to the XY flow direction, and visual inspection of the flow for evidence of glacial realignment and other stratigraphic relationships.

To establish the dip angle and direction of the regional downslope directions, a combination of ArcGIS and MatLab was employed. First, points were selected in approximately 10km intervals forming a square around each lava flow; care was taken to avoid any features such as ridges or craters that would distort the plane of best fit. Second, the XYZ (latitude, longitude, elevation) components for each point were entered into MatLab, and a plane of best fit was generated, yielding the direction of steepest slope, and the dip angle. Third, points at approximately 5km intervals were selected along the center of each lava flow surface, generating a series of line segments. For each segment the azimuthal direction was calculated, and after subtracting out the regional dip direction, the XY plane difference between the flow direction and the regional dip direction. The compilation of each lava flow's line segments then resulted in the average deviation of the lava flow from the dip direction, the standard deviation of the flow itself from the average flow direction, and the XY range of degrees covered by the flow.

The ArcGIS slope profile feature was used for the two remaining slope analyses. For the first one, slope profiles were taken directly to the left, right, and down the center of each lava flow. These were then compared against slope profiles in the direction of steepest decent; here the direction of steepest decent was found by taking the path perpendicular to program calculated contour lines. The second slope analysis took approximately 5 profiles per lava flow across the top of the lava flow, perpendicular to the direction of flow. The resulting data points from these segments were exported to Microsoft Excel spreadsheets, and slope equations and graphs were then generated.

Finally, the flows were visually inspected for regional stratagraphic relationships, and possible evidence of glacial realignment. Notation was made of vents or graben than superposed the lava flows, or possibly caused change in direction. The leading edges in the deviant flow directions were analyzed for steep sides, or any unnatural flow movement. Additionally the tops of the flows were inspected for signs of plucking or scraping indicating previous coverage by ice.

2.3 Aureole Deposit Identification

Visual inspection of the Olympus Mons region reveals several aureole deposit features, whose various origin hypotheses were discussed previously. Aureole deposits to the south and east of the volcanic edifice were selected for dating as they show the least amount of post formation deformation. The three selected were Cyane Sulcii, Sulci Gordii, and Gigas Sulcii located to the northeast, east, and south of the volcano, respectively.

2.4 Crater Retention Age Dating

Image files used for crater counting were obtained from the PIGWAD website, with THEMIS IR Day images covering the most deviant of the lava flows (referenced alternately as "the discordant flow" and Omons 5), and THEMIS VIS images supplying coverage of the aureole deposits, the flexural trough fill area, and one of the semi-deviant lava flows (referenced also as Omons 1). Images were loaded separately into ArcGIS, and then coordinate aligned on top of the colored and hillshaded MOLA data set. The draw line tool measured the diameter of each crater, which was subsequently recorded along with the coordinates in an Excel spreadsheet. This method of identification was limited by the pixel resolution of the data sets, 100m/pixel for THEMIS IR day, and 10m/pixel for THEMIS VIS data. Thus the smallest craters identified for the former were diameter 400m, and diameter 100m for the latter. Craters smaller than 100m were not recorded in the THEMIS VIS data sets because their small size and would not aid in dating the features in question.

Counted craters were also limited to those craters lying directly on the feature to be dated, for example only craters directly on the lava flows or craters on the jagged edges of the aureole deposits. Craters along the edges of the lava flow that clearly superposed the lava flow were also counted. Counting in the aureole deposits was hindered by the poor crater preservation conditions of the aureole deposits. The steep topography and lava infill do not preserve most mid-size craters. The data collected here are also subject to image restraints, which illuminate only a single side of the deposit walls. In all images, care was taken to not include secondary craters, although it is impossible to completely eliminate their inclusion due to human error. Fortunately, the large crater diameter cutoffs exclude most secondary craters from the dating isochrones.

The raw crater diameter data were input into Microsoft Notepad, and saved with the file extension ".diam". Crater retention age isochrones were fit to these data using the CraterStat program provided by the Freie Universität Berlin [Michael and Neukum 2009]. Data were binned using a pseudo-log fit. Several plots for each area were generated, utilizing different ranges of crater diameter. The final set for each area contains the craters that best fit the isochrones and produced the smallest age uncertainties. Due to the statistical nature of crater retention dating, bins with multiple craters were preferred over dates given by single large craters, although this was a personal choice, and differs from some in the crater counting field.

III. Results and Analysis

3.1.1 Lava Flow Populations

The image analysis sought lava flows located around the edges of the visible eastern half of Olympus Mons' flexural trough. The following five flows were selected for analysis based on their length, prominence, and in selected cases, apparent deviance from the expected downhill direction. Once analyzed, the flows were categorized as non-deviant, semi-deviant, and deviant. Non-deviant flows were

observed to follow the topographic downhill direction with an average deviation of no more than 10° from this direction. Semi-deviant flows contained flow segments that varied from the topographic downhill direction by 20°-30°. Portions of these flows followed the expected path, however, each contains certain segments that deviate from the expected downhill direction, with the deviating segment lying very close to the sloped edge of the flexural trough. The flow in the deviant category cuts across the local slope, flowing nearly perpendicular to the expected downhill direction, and varies from said downhill direction by 78° for a majority of the flow path.

Table 1 .**Directional Deviation of Lava Flows**

Flow Name	Regional Dip Direction[1]	Average flow direction[2]	Mean deviation of flow from the regional direction	Standard Deviation of flow from the average flow direction[3]
Omons4 (a)	249.78°	243.07°	22.67°	10.68°
Omons4 (b)	249.78°	236.76°	18.77°	14.88°
Omons4 (c)	249.78°	244.88°	11.56°	6.92°
Omons2 (a)	17.63°	317.74°	59.84°	19.94°
Omons2 (b)	17.63°	335.36°	45.62°	29.70°
Omons2 (c)	17.63°	354.96°	23.59°	15.54°
Omons3 (a)	259.89°	206.13°	53.75°	18.70°

Omons3 (b)	259.89°	228.56°	31.33°	12.67°
Omons1(a)	279.64°	248.97°	33.72°	22.43°
Omons1(b)	279.64°	271.03°	38.65°	24.60°
Omons5	254.37°	332.75°	78.38°	34.13°

[1] Direction of steepest descent measured clockwise in the XY plane
[2] Average direction of flow in measured clockwise in the XY plane
[3] A measure of the sinuosity of the flow, how much it deviates from its average flow direction

3.1.2 Non-Deviant Lava Flow

The lava flow Omons4 (Figure 1) is located on the western flank of Alba Patera, and likely originated from that volcano, or from one of the numerous vents on the volcano's flanks. The flow was selected to serve as a standard. Its path was used to calculate bounds for the movement of unaffected lava flows, and yields bounds for normal sinuosity and deviation from the direction of steepest descent. In the image, the lava flow was divided into three sections: **a** the upper branch of the flow split, **b** the lower branch of the flow split, and **c** the solid original flow before the split point. Both flow segments **a** and **c** exhibit low sinuosity (standard deviation of flow from the average flow direction), the higher standard deviation measurement for flow **b** is a relic of the measuring process at the point where the flow split and translated to the lower trajectory. As shown in Table 1, the Mean Deviation of the Flow for flow **c** , the parent flow is approximately 11.56° which demonstrates how closely the flow follows the current topography. Inspection shows that the daughter flows move in the same direction as the parent flow, strengthening the used of this flow as a standard generally uninterrupted flow, although it is impossible to know definitively the flow's history.

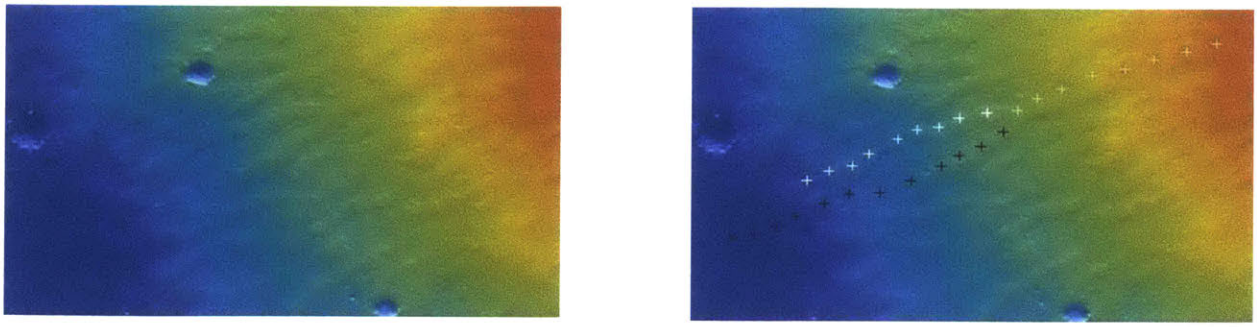

Figure 1a, 1b: **Lava Flow (Omons4).** Figure 1a (left) shows the MOLA topography image of the flow. Figure 1b (right) highlights the flow, and the divisions of it for analysis. Gray Crosses represent **c** , white crosses represent **a** , and black crosses represent **b** .This flow image is centered at 38.8°N 119.1°W. Classified as a non-deviant, and used as a standard.

The lava flow Omons2 (Figure 2) is located to the east of Olympus Mons and to the west of Ascraeus Mons at the saddle point of the two flexural troughs. Due to this strategic placement, one observes the lava initially flowing due north, before turning towards the northwest, depending on the slope of the topography. Within the flow field, three flows were analyzed: **a** on the far left of the image, **b** a flow in the middle left of the region, and **c** the straight flow in the center of the area. The region used to generate the regional downhill direction was carefully chosen to avoid the area affected by the edge of Olympus Mon's flexural trough so as not to corrupt the relative directions for the flow origins. Contour maps of the area indicate that the radically bent flows follow the local topography. Closer analysis of this area of bending reveals that it may represent a shallow ridge built up by repeated lava flows, and thus the odd tail regions are simply the lava fronts that flowed over this ridge, having no real connection to the nearby flexural troughs. The calculations for both **a** and **b** are greatly skewed by the upper bent portion of both flows. Excepting these portions, both flows behave similarly to **c**, with its relatively non-deviant flow path, and mean flow deviation of 23.59°(see Table 1). Although this area is in no way a representative Martian flow, it still falls into the non-deviant category.

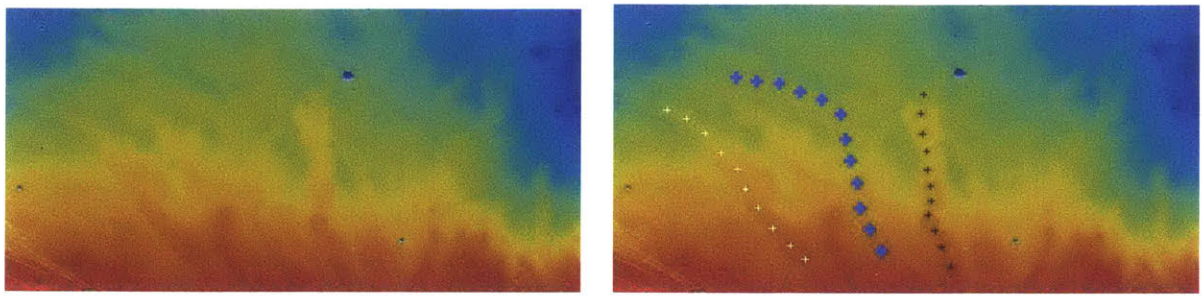

Figure 2a, 2b: **Lava Flow Omons2**. Figure 2a (left) shows the region of the lava flow field taken from MOLA topography. Figure 2b illustrates the different flows analyzed. White crosses represent **a** , blue crosses represent **b** , and black crosses represent **c** . This center of this flow image is 12.4°N 115.4°W. .Omons2 is classified as a non-deviant flow.

3.1.3 Semi Deviant Lava Flow

The lava flow Omons3 (Figure 3) is located to the northeast of Olympus Mons, along the border of the Alba Patera shield and the Olympus Mons flexural trough. Two flows in this region were analyzed: **a** is the shorter upper flow in the image, and **b** is the longer, lower flow. Original inspection suggested these flows were non-deviant because of their low sinuosity, and could perhaps be used as standards. However, comparison of their trajectory with the regional slope plane, revealed distinct differences in the lower portions of both flows. The part of the flow that deviates from the regional plane corresponds with the region that overlays the Olympus Mons flexural trough. Mean Deviations of **a** and **b** are 53.75° and 31.33°, respectively; flow **b** being more statistically significant that flow **a** because the longer flow length allowed for more data points. The deviation near 30° suggests that this region was perhaps topographically different at the time of formation. My current hypothesis is that these flows formed concurrently with the growth of Olympus Mons, hence some of the flexural trough was present, but not as much as at present. Hence, Omons3 is classified as a semi-deviant lava flow.

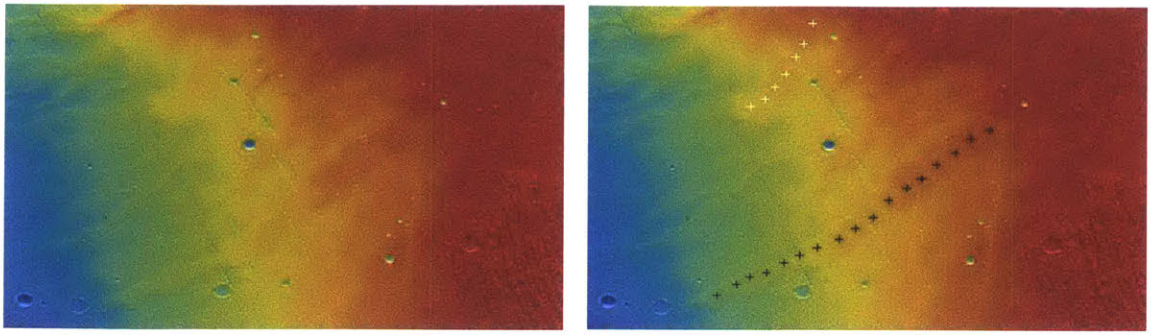

Figure 3a,3b.**Lava Flow Omons3**. Figure 2a (left) displays the MOLA topography of the region. Figure 2b highlights the different flows analyzed. The white crosses represent flow **a** and the black crosses represent flow **b**. The center of this flow image is 31.15°N 116.43°W. Omons3 is classified as semi-deviant lava flow.

The lava flow Omons1(Figure 4) is located directly to the east of Olympus Mons along the rim of the flexural trough. The flow region contains three lava flows that meander across the surface and intertwine, for analysis it was divided into two flows: **a** is the upper traceable flow, and **b** is the lowest portion of the flow system. The flow system has three sections: the upper right section which follows the surface slope, the middle section which changes trajectory away from the surface topography, and the lower left section where the flow path diverges strongly from the surface topography. The overall mean deviation is 33.71° for flow **a** and 38.65° for flow **b**. Although this system has several intertwining flows, the head of the flow implies they all stemmed from the same source, and hence are interpreted to be from the same flow event. Thus, Omons1 is classified as a semi-deviant lava flow.

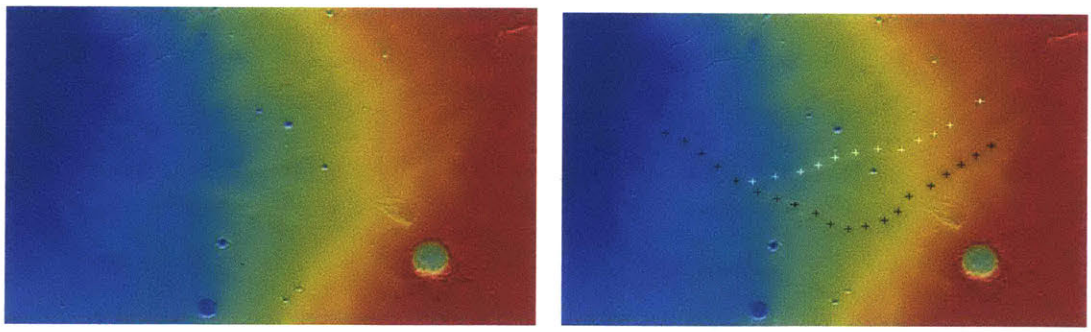

Figure 4a,4b:**Lava Flow Omons1** . Figure 4a depicts the MOLA topography image of the flow system, and figure 4b delineates the different flow branches. The white crosses represent flow **a** and the black crosses represent flow **b**. The center of this flow image is 20°N 120°W. Flow Omons1 is classified as semi-deviant lava flow.

3.1.4 Deviant Lava Flow

The lava flow Omons5 (Figure 5) is located to the northeast of Olympus Mons, just to the north of the steep edge of the flexural trough, but inside the corresponding flexural bulge. The area is dominated by a single large lava flow that flows almost due north, decidedly away from the local downhill direction. The entirety of the flow length displays a mean deviation of 78.38° away from the regional downhill direction. Omons5 is therefore deduced to have formed prior to the current topography. Extending this, Omons5 was emplaced prior to the flexural trough of Olympus Mons and thus prior to Olympus Mons itself, or at least prior to a significant percent of Olympus Mons. With the flow's large deviation from the downhill direction and relatively low sinuosity, it is classified as a deviant flow. This deviant flow serves as an important age marker in the formation history of Olympus Mons.

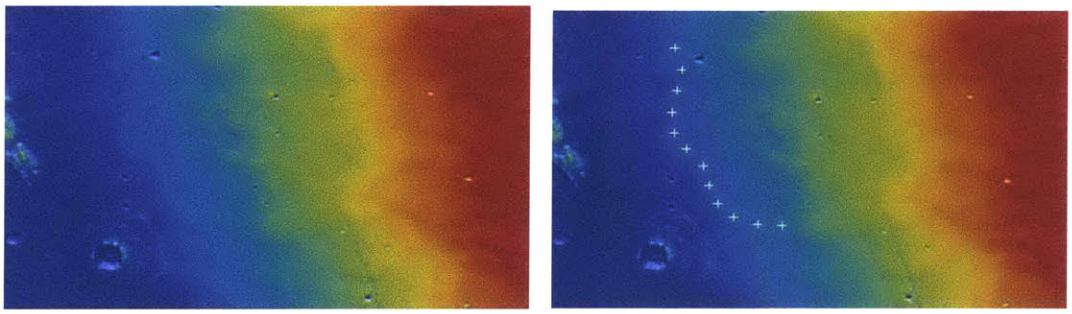

Figure 5a, 5a:**Lava Flow Omons5**. Figure 5a (left) shows the MOLA topography of the lava flow. Figure 5b traces the flow path, with the white crosses overlaying the flow path. Center of the flow image located at 32.6°N 126.46°W. Omons5 is classified as a deviant flow.

3.2.1 Crater Retention Age Dating

Table 2: **Crater Retention Ages**

Region	Image Identification	Diameter Range	$N_{craters}$	Age
Flexural Trough	V13335007	>200m	89	0.156 Ga (+0.025 - 0.028)

Omons5	I10652010	>800m	23	3.67 Ga(+0.05 3 -0.098)
Omons1	V14720012	>1000m	14	3.4 Ga (+0.12 - 0.63)
Cyane Sulci	V12449007	>1000m	5	2.31 Ga (+0.92 - 1.5)
Cyane Sulci, largest crater bin				3.34Ga
Gigas Sulci	V11800007	>800m	15	1.44 Ga (+0.51 - 0.6)
Gigas Sulci, largest crater bin				3.35Ga
Sulci Gordii	V05759015	>800m	8	3.54 Ga (+0.089 - 0.52)

3.2.2 Olympus Mons Flexural Trough

To establish an age for the last period of volcanic activity on Olympus Mons the flexural trough was dated. The site selected was just to the north of Cyane Sulcii, in a region devoid of large scale features. This was preferential as the only features visible in the region were small scale craters and small scale lava flow features as the entirety of the flexural trough had been filled by the most recent period of effusive volcanism from Olympus Mons. The generated isochron (Figure 6) fits the data well, although it is skewed to the younger side based on the prevalence of small craters in the region. Procuring an absolute fit was not a main goal, as several recent studies have dated the flexural trough region and the

flanks of Olympus Mons and obtained a series of ages clustering around 200Ma, which is in concordance with the upper bounds of this age for the flexural trough [Werner 2009].

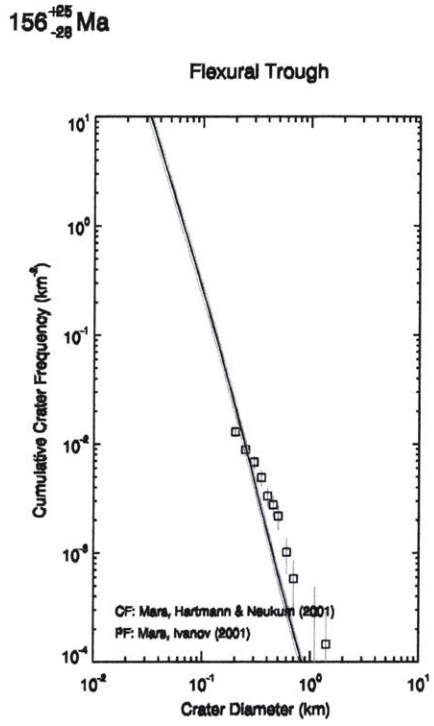

Figure 6. **Olympus Mons Flexural Trough Age**. Pseudo-log binning of all craters D>200m. THEMIS VIS image V13335007. The flexural trough dates to 156 (+25 -29) Ma. The isochron displayed is pulled towards a younger age by many of the smallest craters, omitting these craters moves the age closer to ~200 Ma. Both ages are in concordance with previous ages for the flanks of Olympus Mons (Werner 2009, Neukum 2004).

3.2.3 Lava Flow Omons5

The image used for crater retention age dating the flow Omons5 is THEMIS IR DAY I10652010. Several data sets were searched, but this was the only image that covered a majority of the lava flow region. Craters directly atop the lava flow were counted, as well as, craters that overlap the edges of the flow. The initial plot of all craters showed two distinct crater populations, those of diameter greater than 800m and those with diameter smaller than 400m with a few craters in the intervening sizes. This dichotomy in crater population can be explained by preferential erasure of small craters by resurfacing processes like wind and dust coverage, and then the statistically more likely reformation of small craters through time. By restricting the plot to craters of diameter greater than 800m one obtains a defined pseudo-log regression along the isochron of 3.67Ga (+0.053 -0.098)(Figure 7).

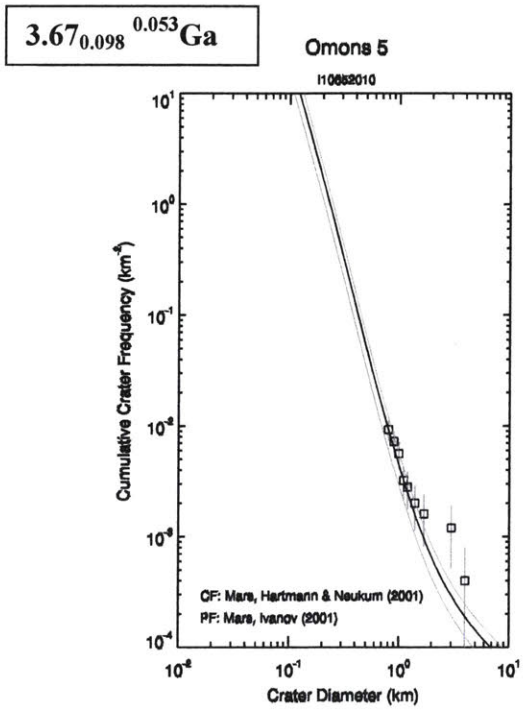

Figure7: **Omons5 Crater Retention Age**. Pseudo-log binning of craters D>800m. THEMIS IR DAY image I10652010. The isochron displays an age of 3.67 (+0.053 -0.098) Ga, and represents a best fit of the largest craters. An isochron passing through the two largest craters bins dates to ~3.68 Ga, although due to the statistical nature of crater retention age dating, the inclusion of the other craters for an age of 3.67 Ga is a more conservative proposition for the age of the lava flow.

3.2.4 Lava Flow Omons1

There was difficulty finding an image that covered the region of Omons1; the image used, V14720012, showed the upper right hand start of the flow region. The region was covered with many branching lava flows of varying thickness. As with Omons5, the smaller craters congregated on the younger isochrones of the graph, and were subsequently omitted in the final graph. The final graph includes craters of diameter 1000m or greater, a fairly sizable population of 14 craters. The age generated was 3.4 Ga (+0.12 -0.63). Looking at Figure 8, one can see that the function outlined by the data points has started to just rollover (the two left-most points), this rollover pushes the age to the younger side. For this reason, I place the age of Omons1 near 3.5Ga, closer to the upper bound of the generated ages. If one takes the upper limit of this age as the age of the lava flow, one arrives at an age mid-way through the formation of

Olympus Mons, a formation history previously postulated from the flow's path, and further analyzed in the discussion section.

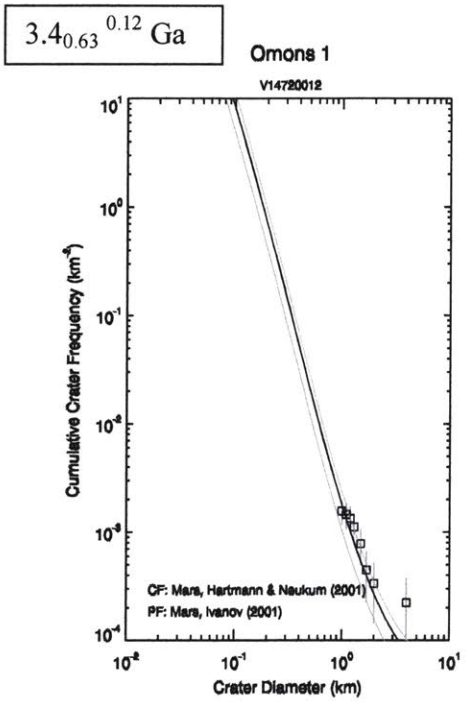

Figure 8: **Omons 1 Crater Retention Age**. Pseudo-log binning of craters D>1000m. THEMIS-VIS image V14720012. The isochron displayed represents an age of 3.4 (+0.12 -0.63) Ga for the lava flow. The far left side of the graph marking the smallest craters begins to turn away from the pseudo-log regression indicating that the actual age is likely slightly older than 3.4Ga, and hence sometime during the formation period of Olymus Mons. This is concordant with the hypothesis that Omons1 is a semi-deviant lava flow emplaced prior to the completion of Olympus Mons and the flexural trough.

3.2.5 Cyane Sulci

Cyane Sulci (Figure 9) is an aureole deposit located to the northeast of Olympus Mons. As noted in the Methods, aureole deposits do not preserve craters well, and as such, finding an image with enough craters to provide a reasonable age was difficult. THEMIS-VIS image V12449007 provided a significant amount of data. The generated age based on craters with diameter greater than 1000m was 2.31Ga (+0.92 -1.5). However, the largest crater bin dated to 3.34Ga, which is both near to the upper bound for the age, as well as, near in age to dates garnered from the other aureole deposits. Crater retention age dating relies on the statistical frequency of crater impacts. Given that the aureole deposits preserve only a fraction of the crater impacts, and of that fraction only a select number are viewable from select camera angles, one can infer that the crater record presented is incomplete, and that a number of larger craters are not being considered. For these reasons, I date Cyane Sulci based on the age of the largest crater bin. This reasoning

also applies to Gigas Sulci, where there is also a sizable difference in the general crater population, and the largest crater bin.

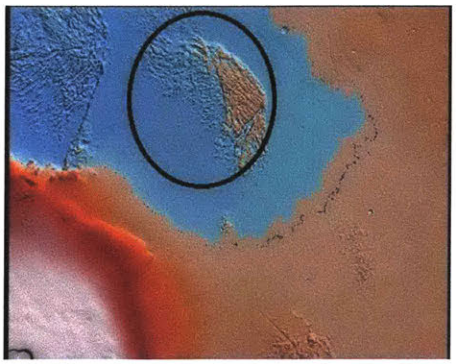

Figure 9: **Aureole Deposit Cyane Sulci.** The deposit is centered at 128.7°W 25.7°N. Image was generated with MOLA topography data rastered in Gridview.

2.31 $_{1.5}^{0.92}$Ga
largest bin 3.34Ga

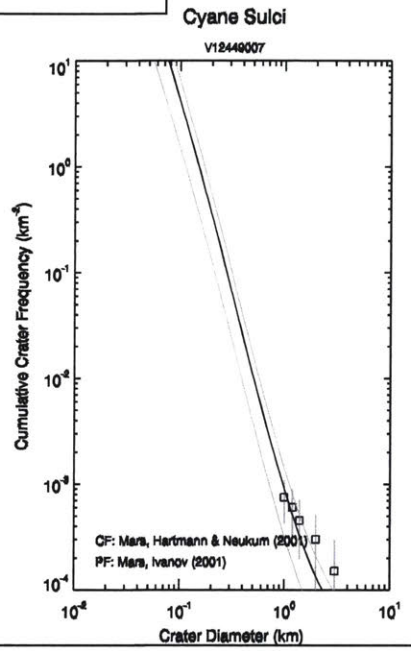

Figure 10: **Crater Retention Age of Cyane Sulci**. Pseudo-log binning of craters D>1000m.. THEMIS-VIS image V12449007. The isochron displayed indicates an age of 2.31 (+0.92 -1.5)Ga. Note, however, the outlying largest crater bin, age 3.34Ga. This is the age taken for Cyane Sulci. Aureole deposits do not preserve craters well, and hence gaps in the crater record make dating from just isochrones imprecise. As is common in crater retention dating, the age of the oldest craters is preferentially used with the remainder of the crater record held suspect to crater altering resurfacing processes.

3.2.6 Gigas Sulci

Gigas Sulci (Figure 11) is an extensive aureole deposit located to the south of Olympus Mons. As with the other aureole deposits, it was difficult to procure an image with an adequate crater record, however, the THEMIS-VIS image V11800007 provided enough craters to be useful. The crater retention age for all craters with diameter greater than 800m is 1.44 Ga (+0.51 -0.6). The largest crater bin for this aureole deposit date to 3.35Ga, however. The large gap in the crater record between the largest crater bin, and the rest of the craters suggest resurfacing on the steep slopes of the aureole deposit, artificially lowering the

age of Gigas Sulci. Thus, as with Cyane Sulci, the date taken for Gigas Sulci comes from the age of the largest craters, here 3.35G.

Figure 11: **Image of Gigas Sulci.** The deposit is centered at 127.8° 9.88°N. The image was generated using MOLA topography data in the Gridview program.

$1.44_{0.6}^{0.51}$ Ga
Largest Bin 3.35 Ga

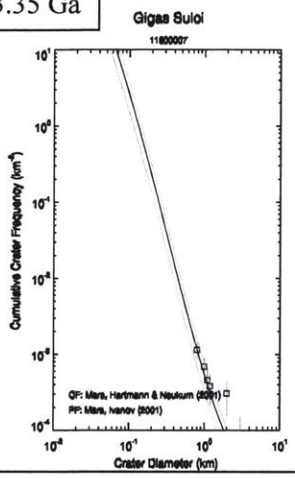

Figure 12: **Crater Retention Age of Gigas Sulci**. Pseudo-log binning of crater D>800m. THEMIS-VIS image V11800007. The isochron displays an age of 1.44 Ga, however, this is vastly separated from the largest crater bin of 3.35 Ga. As noted in the other aureole deposits, the age of the oldest/largest craters is used for dating the deposit.

3.2.7 Sulci Gordii

The aureole deposit Sulci Gordii (Figure 13) is located due east of Olympus Mons. The floor of the deposit exhibited a perceived higher level of lava fill than the other two aureole deposits that were examined. Craters with diameter greater than 800m from THEMIW-VIS image V05759015 were used to generate the displayed isochron, and the age of 3.54 Ga (+0.089 -0.52). As seen in Figure 14, the age generated for Sulci Gordii represents a compromise between two pseudo-log functions, one above, and one below the displayed isochron. Following the interpretation of the previous aureole deposits, we will follow the age closer to the largest crater bin, here younger than the given isochron, thus pushing the age of Sulci Gordii closer to the ages of the other aureole deposits, near 3.35Ga.

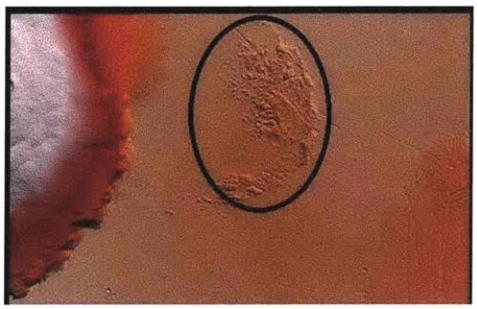

Figure 13: **Image of Sulcii Gordii**. The aureole deposit is centered at 125.5°W 18.9°N . The image was generated with MOLA topography in the Gridview program.

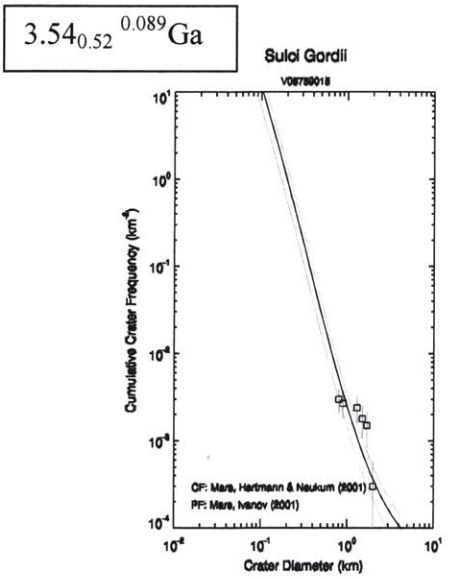

Figure 14: **Crater Retention Age of Sulci Gordii**. Pseudo-log binning of craters D>800. THEMIS-VIS image V05759015. The isochron displays an age of 3.54 (+0.089 -0.52) Ga. Notice the isochron is skewed towards older ages by a few of the middle size crater bins, following the procedure of dating based on the largest craters, the age for Sulci Gordii is slightly younger than 3.54 Ga, and likely closer to 3.48 Ga.

IV. Discussion

Compiling the results of crater retention age dating from the previous section, a timeline for the formation of Olympus Mons emerges. At 3.67Ga there was no more than a small percentage of Olympus Mons present. The volcano then built itself up until approximately 3.4Ga when the aureole deposits formed as a result of brittle failure in the crust caused by the loading of Olympus Mons. Olympus Mons continued to undergo periodic eruptions until 150Ma, although these contributed very little to the edifice bulk.

4.1 Evidence against Glaciation

In order for lava flow Omons5 to provide a viable age marker in this method, the flow must have flowed freely during initial emplacement, and not have been deflected by surface features. Terrestrial lava flows can be deflected by interactions with glaciers, and thus there can be speculation that Martian glaciations diverted Omons5. A recent study of fan-shaped deposits on the northwestern flanks of the Tharsis Montes suggests each of these areas are the result of Amazonian glaciations [Shean et al 2005]. This research does not address whether Olympus Mons experienced glaciation on its flanks; correspondingly, no analysis was carried out on the immediate flanks of Olympus Mons or the large deposits directly to the northwest of the volcano.

The lava flow Omons5 itself, does not exhibit any signs of being deflected as a result of abutting a glacier during its formation time. Lava flows that are deflected by glaciers display a sharp well defined edge with a high elevation from the ground where the lava contacted the ice [Shean et. al. 2005]. The leading deflected edge of Omons5 has a natural unobstructed flow pattern, marked by an irregular edge, showing no signs of having ever abutted another surface. Indeed, the surface of the flow itself is not parallel to the planet surface, but rather inclined in the current downhill direction. This further supports the assertion that the lava flow formed and cooled, the surface was reoriented under the influence of Olympus Mons' flexural trough.

4.2 Aureole Deposit Formation Theory

The use of the aureole deposit ages as a marker for the end of Olympus Mons' bulk formation uses the assumption that aureole deposits are a consequence of mass crustal failure in response to lithosphere loading. This model for rapid crustal fractionation and aureole formation is covered extensively in McGovern's 2004 paper, *Olympus Mons aureole deposits: New evidence for a flank failure origin*[McGovern et.al. 2004]. Alternative theories for aureole deposit formation include massive

landslides from the flanks of Olympus Mons [Lopes et al. 1982], and long term spreading of sediments at low strain rates driven by gravity [Francis and Wadge, 1983; Tanaka, 1985]. The crater record provided by the aureole deposits favors a rapid formation. As seen in Figures 13 and 10, the deposits display continuous crater histories with a few very large, old craters progressing through a compliment of smaller craters, including uncounted craters in the floor space between deposit ridges. If the ridges had formed slowly, one would expect a discontinuous crater size history, as ridges of different ages were formed, or craters were erased in the process of continual ridge formation. It is difficult to wholly discount the possibility of small-scale, intermittent landslides from the surface of Olympus Mons' flanks contributing to the bulk of the aureole deposits, especially the deposits on the northwest flanks of the volcano. However, these are to be considered distinctly different from the massive crustal movements from the flanks that characterized the aureole deposit formation. To avoid this potential contribution of non related rockslides as much as possible, aureole deposits separated from direct basal contact were selected. The fact that deposits exist at a distance of several kilometers from the base of the volcano also supports the assumption that landslides from the flanks of Olympus Mons were not a contributing factor in their formation.

4.3 Flexural Modeling

The timeline for Olympus Mons formation is further refined by establishing how much of the volcanic edifice could have been present at the time of Omons5 emplacement without disrupting the flow's initial trajectory. The following flexural models and results are credited to my colleague R.J. Isherwood, whose work was presented in tandem with this work at the Lunar and Planetary Science Conference 2011, further details of which can be found in LSPC Abstract #2202, and in Appendix A. After establishing the lithospheric thickness, the bulk of Olympus Mons was increased linearly. The region surrounding Omons5 was monitored for slope changes in the direction of Olympus Mons corresponding to flexural trough formation. The topographic distortion noted indicates the percent increase in slope for the Olympus Mons downhill direction verses the slope in the original flow direction. Thus, a 10% change

indicates that the slope in the direction of Olympus Mons imposed by the flexural trough is 10% steeper than the slope in the original flow direction. The lower bound for flow redirection was set at 10% slope difference, and the upper bound was set at 45%. Thus, at the time of Omons5 emplacement, 10-42% of Olympus Mons could have been present. This is an exaggeratedly large range, for the flow would almost certainly have redirected well before a 45% slope difference. We postulate the upper bound for Olympus Mons bulk present at Omons5 formation was 20% [R.J.Isherwood, personal correspondence].

4.4 Olympus Mons Eruption Rate

Calculations of the present volume of Olympus Mons carried out using the Gridview program yield approximately $4.4\times10^{6}km^{3}$. The ages given by the crater dating show a minimum edifice construction of 14_{-19}^{+33} Myr , based on the constraints of 3.67-3.53Ga. A more conservative estimation for the edifice construction time is 27_{-21}^{+47}Myr, based on the ages of 3.67-3.4Ga. The eruption rate for the shorter time period is ~0.31 km^{3}/yr, and the eruption rate for the longer formation period is ~0.16 km^{3}/yr. Average terrestrial hotspot volcano eruption rates are 0.03-0.1 km^{3}/yr [Campbell and Griffiths, 1990] with the Hawaiian volcanoes demonstrating eruption rates at the high end of this estimation between 0.085 to 0.155 km^{3}/yr [Clague & Dalrymple, 1987]. The eruption rates for Olympus Mons are higher than terrestrial rates, although not egregiously so; in fact, the postulated eruption rate for the more reasonable formation period falls within the upper bounds of terrestrial hot spot volcano eruption rates. A simple explanation for the higher eruption rates is the gravity difference between the Earth and Mars. Wilson and Parfitt demonstrated that using simple gravity scaling and considerations for local rock strength, one would expect eruption rates on Mars to be approximately 5 times greater than terrestrial eruption rates [Wilson and Parfitt, LPSC 1989].

4.5 Mantle Plume Origin

Uncertainty still surrounds the formation mechanism of Olympus Mons, I propose it is a hot spot volcano formed by a mantle plume. Terrestrial mantle plumes arise when the hotter core heats the contacted mantle at the core mantle boundary, lowering the density of the newly heated mantle; this mantle then rises through the surrounding denser mantle material [Campbell, 2007]. As the plume rises it assumes a characteristic shape with a mushroom head and a trailing tail that extends back to the core mantle boundary [Griffiths and Campbell, 1990]. The plume head then erupts as low viscosity flood basalt which covers a large area surrounding the volcano. The plume tail then erupts in a more constrained fashion, with higher viscosity lava, building the main edifice of the volcano [Griffiths and Campbell, 1990].

The results from this study combined with lava flows noted in other studies construct a broad timeline for Olympus Mons formation that coincides with the stages of mantle plume volcano formation. Werner notes mesa like formations on the far western flanks of Olympus Mons that date to 3.83 Ga [Werner, 2009]. This date corresponds to the single largest crater bin, and as with our treatment of the aureole deposits, the remaining crater trend is dismissed as a remnant of later resurfacing activity. These flows perhaps represent the earliest volcanic activity in the region, a proto-Olympus Mons, although based on their age, it is unlikely they are of the same volcanic episode as Olympus Mons itself. Several lava flows emanating from the Olympus Mons region, located at the edge of the Amazonis Planitia and emanating from under the westernmost aureole deposits [Fuller and Head, 2002]. These lava flows may represent the flood basalt stage of plume head eruption. They predate the aureole deposits, and extend beyond the immediate vicinity of the Olympus Mons region, but the flows are well inside the flow distance of flood basalts. Terrestrial flood basalts in the North Atlantic are observed to extend 2400km, the diameter of the plume head [Campbell, 2007].

The time interval between plume head emergence and edifice construction by the plume tail must also be addressed. Analysis of the terrestrial Parana flood basalt province places formation at 1 Myr [Campbell et

al., 1992 and Gallet et al., 1989]. The interval between the western flank mesas and Omons5 emplacement is 16 Myr, longer than seen in terrestrial flows. This assumes that no flood basalts were erupted after the 3.83 Ga mark, and that Olympus Mons did not begin to form until after Omons5, hence it is unlikely that the flow Werner 2009 notes in the Amazonis Planitia are from the Olympus Mons formation plume. Without a crater retention age for the flow noted in Fuller and Head 2002, it is unable to be categorically placed as early stage flood basalt, or a later flow. Given the vast amount of volcanic and geologic activity in the region surrounding Olympus Mons it is unlikely that a single lava flow associated solely with the flood basalt stage will be found. Moreover, it is more likely that the edifice of Olympus Mons is built upon the flood basalt province itself. . Little is known about the composition and viscosity of the Olympus Mons lava and how lava flows on Mars, allowing for the possibility that the flood basalts themselves began to erect the edifice of Olympus Mons instead of simply spreading out along the planet surface as they do in terrestrial models [Elkins-Tanton, personal correspondence]

Following head effusion, the tail of the mantle plume proceeded to erect the bulk of Olympus Mons over a period of approximately 26 Myr. The Leeward isles of the Hawaiian-Emperor Seamount chain date to 27.7 Myr with eruptions presently ongoing [Clague and Dalrymple, 1987]. Mars, however, lacks plate tectonics, so both plume and head were effused in the same crustal location, as opposed to forming a series of volcanoes like the Hawaiian chain. Aureole deposit formation as a result of cataclysmic failure of the crust under the load of Olympus Mons also favors a faster loading time as it suggests the lithosphere did not have sufficient time to compensate for the growing load before fracture occurred.

Although this model proposes the bulk of Olympus Mons construction was completed by 3.4Ga, there is a plethora of evidence indicated that volcanic activity continued in the region until approximately 150 Myr. The caldera and flanks of Olympus Mons have been dated to 150-200 Myr, and this study confirmed theses dates with an age of 156_{-28}^{+25} Myr [Werner, 2009 and Neukum et. al., 2004]. If Olympus Mons were to have erupted at the same rate for the entire period between 3.67 and 0.15 Ga, the eruption rate

would be approximately 0.00125 km^3/yr. This dramatic difference in eruption rate compared with an eruption rate of ~0.16 km^3/yr suggests that the later volcanism is the result of a different mechanism than the original mantle plume. It is likely that Olympus Mons provided a ready plumping system for any subsequent small-scale volcanic activity in the region, or provided a conduit for transporting small bits of mantle melt to the surface where they then resurfaced the flanks of Olympus Mons and filled the flexural trough. The Tharsis region hosts numerous vents in addition to the younger Tharsis Montes supporting continued volcanic activity in the Olympus Mons region after bulk formation had ceased.

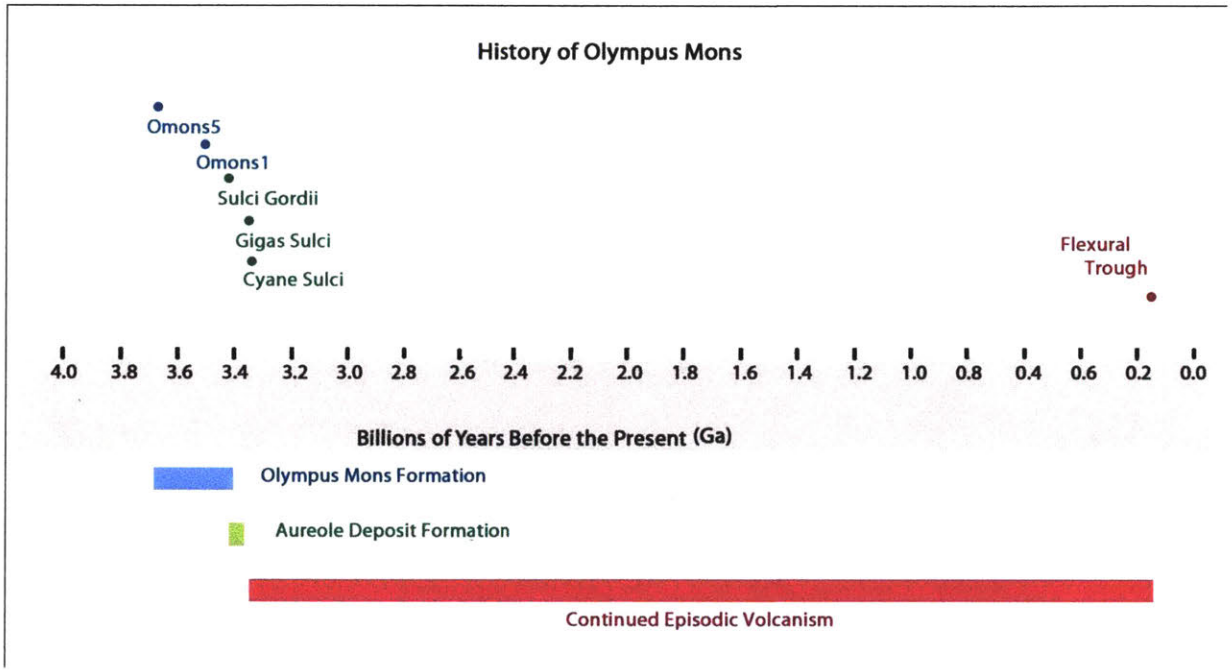

Figure 14: **History of Olympus Mons Timeline**. The upper portion of the timeline charts the ages presented in this work for pertinent lava flows, aureole deposits, and the flexural trough fill. The bottom portion of the timeline delineates the broad periods of Olympus Mons formation history. We see that Olympus Mons formed quickly, early in Martian history, but that has experienced volcanic activity until the near present. The exact mechanism for this continued volcanism is unknown. The activity likely represents separate magma movements using the existing plumbing of Olympus Mons, and not continued activity of the initial Olympus Mons mantle plume.

V. Conclusions

As illustrated by paleo-topography, Olympus Mons was built during the early Hesperian between 3.67 and 3.4 Ga, likely as the result of a mantle plume. Lava flows whose paths are discordant with the present day topography created by the Olympus Mons flexural trough imply emplacement prior to the trough and Olympus Mons itself, and thus yield a constraint on the onset of Olympus Mons construction. Aureole deposits resulting from crustal fracture under the load of Olympus Mons place a constraint on the end of Olympus Mons bulk construction. Combined, these dates yield a ~26 Myr construction phase for Olympus Mons with an average eruption rate of 0.16 km^3/yr. Olympus Mons can be modeled as a mantle plume volcano: the plume head effusing flood basalts that covered the regional plain and began edifice construction with the remainder of Olympus Mons built up relatively quickly by the rising plume tail. Both the construction time and eruption rates of Olympus Mons are similar to those of the Hawaiian Island chain, the most prominent terrestrial plume volcano.

Appendix A: Flexural Loading

The first analysis in the flexural loading model established the lithosphere thickness for the Olympus Mons region (Johnson et.al. 2000). A thin-shell spherical harmonic loading model was employed. Crustal thicknesses of 75km, 85km, and 100km were modeled under the current volume of Olympus Mons. The resulting flexure profiles in the region of Omons5 were recorded and compared to the actual topographic profile of the region. A lithospheric thickness of 85km displayed the closest fit. This model uses the overly simplified assumption of uniform crustal thickness; thus underestimating the width of the flexural trough and providing upper bounds for the subsequent analysis of Olympus Mons bulk.

The analysis of flow redirection operated between and upper and lower bound of flow redirection. In the extreme upper case, the slope in the direction of the flexural trough equals the slope in the flow's natural direction. This would cause the flow to reorient 45° azimuthally towards the flexural trough direction. The lower case assumed that a slope in the flexural trough direction that was 10% (natural variability, sinusodosity, of the previously analyzed lava flows) of the slope in the flow's natural direction would reorient the flow. These bounds were marked, and the corresponding percent bulk of Olympus Mons was charted, ranging between 10% volume to 42% present volume.

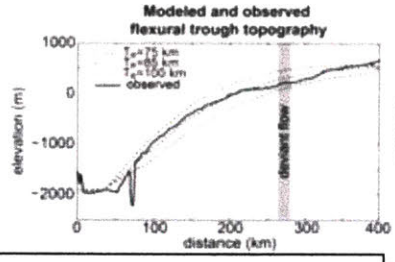

Figure 16: **Flexural Trough Lithospheric Thickness**. Models for lithosphere thickness corresponding to 75km, 85km, and 100km plotted with the observed topography of the flexural trough. A thickness of 85km fits closely with the observed. Variations in the model and observed topography arise from the simplicity of the model assuming uniform crustal thickness, as well as the uncertain geophysical history of the region. Image credit R.J. Isherwood.

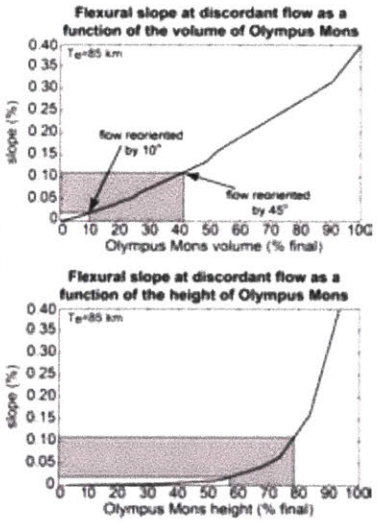

Figure 17: **Flexural Slope at Omons5 and Corresponding Olympus Mons Volume.** The upper graph notes the percent volume of Olympus Mons at the points where it creates a 10% and a 45% slope difference between the natural flow slope direction and the direction of Olympus Mons. The lower graph notes the same percent slope difference plotted against percent of Olympus Mons final height. Both cases are extreme upper and lower bounds, with the actual percent of Olympus Mons that would have redirected Omons5 likely residing around 20%.

References:

Campbell I. H. (2007) The Great Plume Debate: Testing the Plume Theory. *Chemical Geology. 241.* (3-4).153-176.

Campbell I. H. and R. W. Griffiths (1990). Stirring and structure in mantle starting plumes. *Earth and Planetary Science Letters. 99.* 66-78.

Campbell et al. (1992) Synchronism of the Siberian traps and the Permian–Triassic boundary, *Science. 258.* 1760–1763.

Clague D.A. and G. B. Dalrymple(1987). The Hawaiian-Emperor volcanic chain. *U.S. Geologic Survey. Prof. Paper.* (1350) 5-54.

Francis, P.W., and G. Wadge, (1983) The Olympus Mons aureole: Formation by gravitational spreading. *Journal of Geophysical Research, 88,* 8333–8344.

Fuller E. R. and J. W. Head (2002) Amazonis Planitia: The role of geologically recent volcanism and sedimentation in the formation of the smoothest plains on Mars. *Journal Of Geophysical Research 107,*(E10) 5081, doi:10.1029/2002JE001842

Gallet et al. (1989) Duration of Deccan trap volcanism — a statistical approach, *Earth and Planetary Science Letters. 93.* 273–282.

Johnson et. al. (2000) Lithospheric Loading by the Northern Polar Cap on Mars. *Icarus.144.* 313-328. doi:10.1006/icar.1999.6310.

Liu L. and M. Gurnis (2010) Dynamic Subsidence and Uplift of the Colorado Plateau. *Geology, 38.* 663-666.

Lopes et al., (1982) Further evidence for a mass movement origin of the Olympus Mons aureole. *Journal of Geophysical Research. 87.* 9917–9928.

McGovern et. al. (2004) Olympus Mons aureole deposits: New evidence for a flank failure origin. *Journal of Geophysical Research. 109.*(E08008) doi:10.1029/2004JE002258.

Michael G. and G. Neukum (2009) Surface Dating: Software Tool For Analyzing Crater Size-Frequency Distributions Including Those Showing Partial Resurfacing Events. *Lunar and Planetary XXXIX.*1780.

Neukum et. al. (2004) Recent and episodic volcanic and glacial activity on Mars revealed by the High Resolution Stereo Camera. *Nature. 432.* (23/30 December 2004).

Shean, D. E., J. W. Head, and D. R. Marchant (2005), Origin and evolution of a cold-based tropical mountain glacier on Mars: The Pavonis Mons fan-shaped deposit, *Journal of Geophysical. Research, 110.* (E05001) doi:10.1029/2004JE002360.

Tanaka K.L. (1985) Ice-lubricated gravity spreading of the Olympus Mons aureole deposits. *Icarus 62* 191–206.

Werner S. C. (2009) The Global Martian Volcanic Evolutionary History. *Icarus. 201.* 44-68.
Wilson L. and E. A. Parfitt (1989) The Influence of Gravity on Planetary Volcanic Eruption Rates: A Reappraisal. *Abstracts of the Lunar and Planetary Science Conference. 20.* 1213.